# NASA

## Technical Memorandum 80332

# An improved Scheme
# for the Remote Sensing
# of Sea Surface Temperature

## G. Dalu, C. Prabhakara,
## R. C. Lo and M. J. Mack

**JULY 1979**

# AN IMPROVED SCHEME FOR THE REMOTE SENSING

# OF SEA SURFACE TEMPERATURE

G. Dalu*, C. Prabhakara
Laboratory for Atmospheric Sciences (GLAS)
NASA/Goddard Space Flight Center
Greenbelt, Maryland 20771


R. C. Lo, M. J. Mack
Computer Sciences Corporation
Silver Spring, Maryland 20910

*NAS/NRC Research Associate on leave from C.N.R., Istituto di Fisica della Atmosfera, Rome Italy.

# CONTENTS

# TABLES

# ILLUSTRATIONS

# AN IMPROVED SCHEME FOR THE REMOTE SENSING
## OF SEA SURFACE TEMPERATURE

G. Dalu*, C. Prabhakara
Laboratory for Atmospheric Sciences (GLAS)
NASA/Goddard Space Flight Center
Greenbelt, Maryland 20771

R. C. Lo, M. J. Mack
Computer Sciences Corporation
Silver Spring, Maryland 20910

## ABSTRACT

A radiometer which has two channels in the 11 to 13 $\mu$m window region, has been proposed for inclusion on the forthcoming NOAA satellites. It will be useful in estimating the sea surface temperature to within an accuracy of 1°C. But this study shows that this accuracy could be improved to within 0.3°C, if an independent estimate of total precipitable water vapor is available. In order to remotely sense the total precipitable water vapor, a broadband channel in the 18 $\mu$m water vapor band should be introduced in addition to the two channels in the 11 to 13 $\mu$m window region. With these three channels the total water vapor could be estimated over oceans, which would improve the accuracy of the sea surface temperature estimation. In addition the effect of the surface emissivity is taken into account in this scheme.

*NAS/NRC Research Associate on leave from C.N.R., Istituto di Fisica della Atmosfera, Rome, Italy.

# AN IMPROVED SCHEME FOR THE REMOTE SENSING
# OF SEA SURFACE TEMPERATURE

## INTRODUCTION

Radiometric measurements in the 8 to 13 $\mu$m water vapor window are generally used for re-mote sensing of the sea surface temperature (SST). The brightness temperature corresponding to the measured radiances is always lower than the SST, because of the atmospheric water vapor absorp-tion. A simple approach based on climatological data for atmospheric water vapor content as a function of latitude and season was developed to correct for such absorption (Smith et al., 1970). However since the variability of water vapor in the atmosphere is comparable to its mean value, this climatological data set information is inadequate. The water vapor information for the SST has to be derived from simultaneous independent measurements.

In a previous study, Prabhakara et al. (1974), hereafter referred to as PDK, used the differential absorption properties of the water vapor to determine the water vapor absorption correction from two channels in the 11 to 13 $\mu$m window region (the Split Window Technique, SWT). The RMS error of SST estimated with the SWT, was found to be about $\pm 1.3^\circ$C when compared with ship measurements.

Recently Prabhakara et al. (1979) demonstrated that the total water vapor content can be de-termined from the water vapor line strength in the 9 $\mu$m region, with an accuracy of about $\pm 0.3$ g/cm$^2$. With this information, it is possible to improve the split window technique by removing some of its approximations.

In this study we have considered a broad band ($\sim$ 1 $\mu$m) radiometer channel in the 18 $\mu$m re-gion to derive the precipitable water vapor information (Wark et al., 1974). An instrument with this

1

channel is easier to incorporate into space flights than a spectrometer and can have higher spatial resolution. Since the surface emissivity effect on SST estimation can not be neglected when high accuracy is desired, an empirical correction was introduced to take this effect into account.

# RADIATIVE TRANSFER SIMULATIONS

Assuming local thermodynamic equilibrium and no scattering, the radiative intensity $I(\nu)$ emerging at the top of the atmosphere is

$$I(\nu) = B(\nu, T_s)\, \tau(\nu, p_0) + \int_{\tau(\nu, p_0)}^{1} B[\nu, T(p)]\, d\tau(\nu, p) \tag{1}$$

where $T_s$    surface temperature, K;

      $p_0$    surface pressure, mb;

      p    pressure at any height, mb;

      $\nu$    wave number, $cm^{-1}$;

      T    temperature, K;

      B    Planck intensity, erg $cm^{-1}$ $sr^{-1}$ $s^{-1}$;

      $\tau$    transmission from any pressure level p to the top of the atmosphere.

Here, surface emissivity is assumed to be unity. The effect of the actual emissivity will be examined separately.

Equation (1) may be simplified as

$$I(\nu, T) = B(\nu, T_s)\, \tau(\nu, p_0) + \bar{B}(\nu, \bar{T})\, [1 - \tau(\nu, p_0)] \tag{2}$$

where $\bar{B}(\nu, \bar{T})$ is the weighted mean Planck emission of the atmosphere:

$$\bar{B}(\nu, \bar{T}) = \frac{\displaystyle\int_{\tau(\nu, p_0)}^{1} B[\nu, T(p)]\, d\tau}{\displaystyle\int_{\tau(\nu, p_0)}^{1} d\tau} \tag{3}$$

and $\bar{T}$ is the equivalent radiative temperature of the atmosphere. The Planck function B can be expressed as

$$B(\nu, T) = B(\nu, T_s) + \frac{\partial B(\nu, T_s)}{\partial T}(T - T_s) \tag{4}$$

This approximation is appropriate over a small temperature range and a narrow wave number interval. Equation (2) now becomes

$$T_s - T(\nu) = [1 - \tau(\nu)] \; [T_s - \overline{T}(\nu)] \tag{5}$$

where $T(\nu)$ is the brightness temperature and $\overline{T}(\nu)$ is the equivalent radiative temperature of the atmosphere. If measurements are made in two channels, one centered around 11 $\mu$m and the other centered around 13 $\mu$m, and if $\tau(\nu)$ can be obtained from an independent estimate of the total water vapor content w, i.e.

$$\tau(\nu) = f_\nu (w) \tag{6}$$

we have two equations with three unknowns; $T_s$, $\overline{T}_{11}$ and $\overline{T}_{13}$. But $\overline{T}_{11}$ and $\overline{T}_{13}$ are not independent.

In order to study the relationship $\tau(\nu) = f_\nu(w)$ and the manner in which $\overline{T}(\nu)$ changes as a function of wave number for different atmospheric conditions, we have developed a radiation computational scheme for the radiative transfer equation (1).

The transmission function, $\tau$, of the water vapor needed in these calculations is taken to be the product of three components: $\tau_l$ associated with water vapor lines, $\tau_p$ produced by the continuum due to foreign broadening, and $\tau_e$ resulting from the e–type absorption (Bignell, 1970). The transmission function of the water vapor lines $\tau_l$ is derived using a multiple regression scheme similar to the one proposed by Smith (1969). The method also incorporates the details of the foreign broadening and the e–type absorption (Kunde and Maguire, 1974).

4

Several temperature and humidity profiles were used in this computational scheme to simulate the radiative response of the atmosphere. In each one of these temperature profiles the SST was changed in steps of $5°K$, to cover the range 273 to $308°K$, while the temperature gradient was kept constant and equal to the temperature gradient of the U.S. Standard Atmosphere (U.S. Standard Atmosphere, 1976). The relative humidity profile described in Manabe and Wetherald (1976) was used in all of these simulations.

The relationship (6) obtained from these simulations is shown in Figure 1 for two channels, 915 to 976 $cm^{-1}$ (11 $\mu m$) and 776 to 845 $cm^{-1}$ (13 $\mu m$).

Furthermore it was found that

$$T_s - \bar{T}_{13} = C (T_s - \bar{T}_{11}) \tag{7}$$

where $C = 1.2$ is a constant (Figure 2).

If we combine Equation (7) with the equations derived from (5) for the same two channels, we have

$$T_s = T_{11} + g(w) (T_{11} - T_{13}) \tag{8}$$

where

$$g(w) = \frac{1 - \tau_{11}}{1.2 (1 - \tau_{13}) - (1 - \tau_{11})} \tag{9}$$

In Figure 3 the relationship between g and w is shown. Now, if w is available from an independent measurement, we can calculate g(w) using the relationship shown in Figure 3, and then calculate the corrected SST from Equation (8). PDK used $g(w) = constant = 1.195$, which is the value that corresponds to about $w = 3.7$ $g/cm^2$. This implies an overcorrection (undercorrection) of SST when w is smaller (larger) than 3.7 $g/cm^2$.
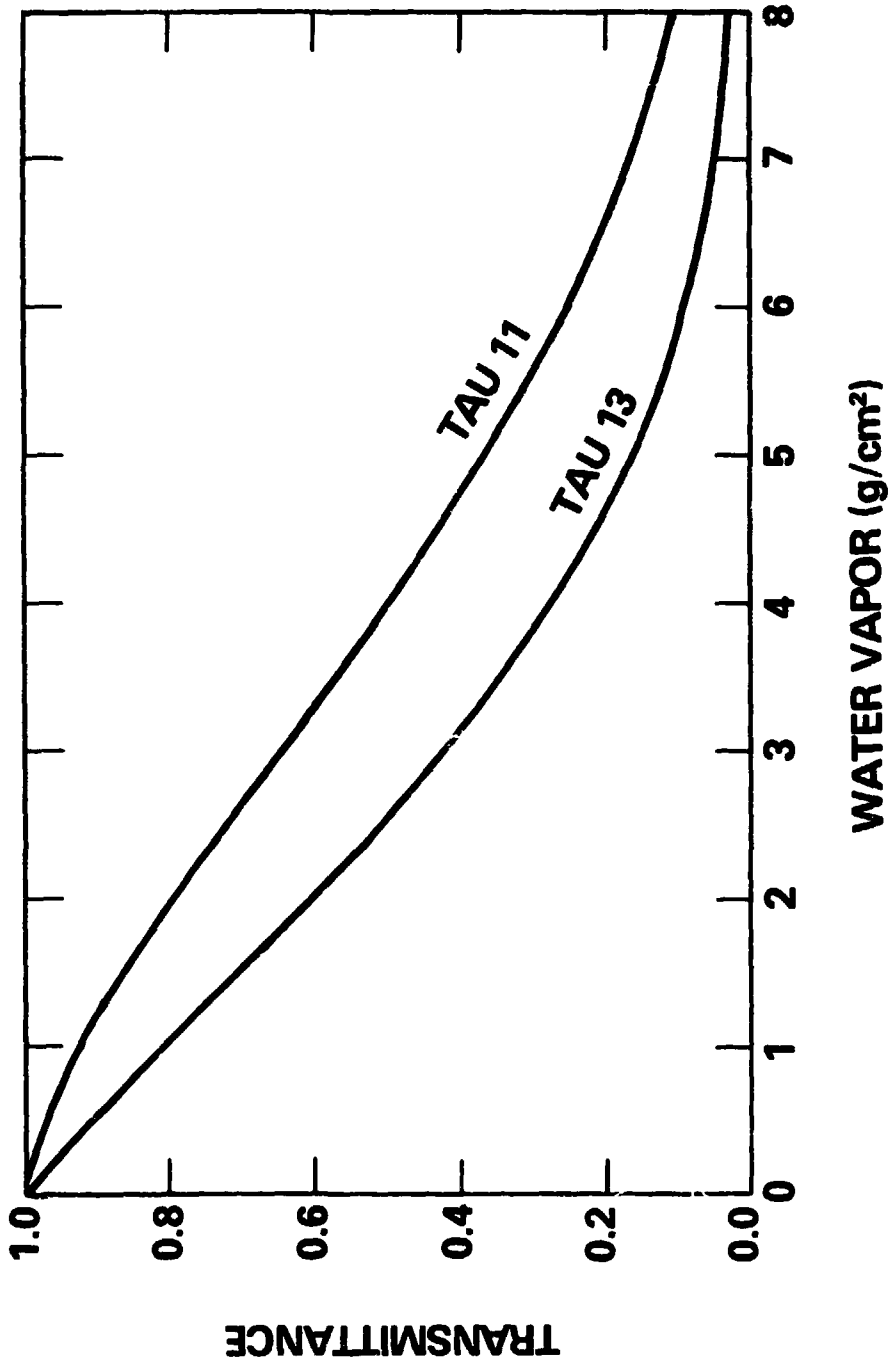
Figure 1. Total transmittance for two window channels as a function of atmospheric water vapor content, calculated for average atmospheric conditions.
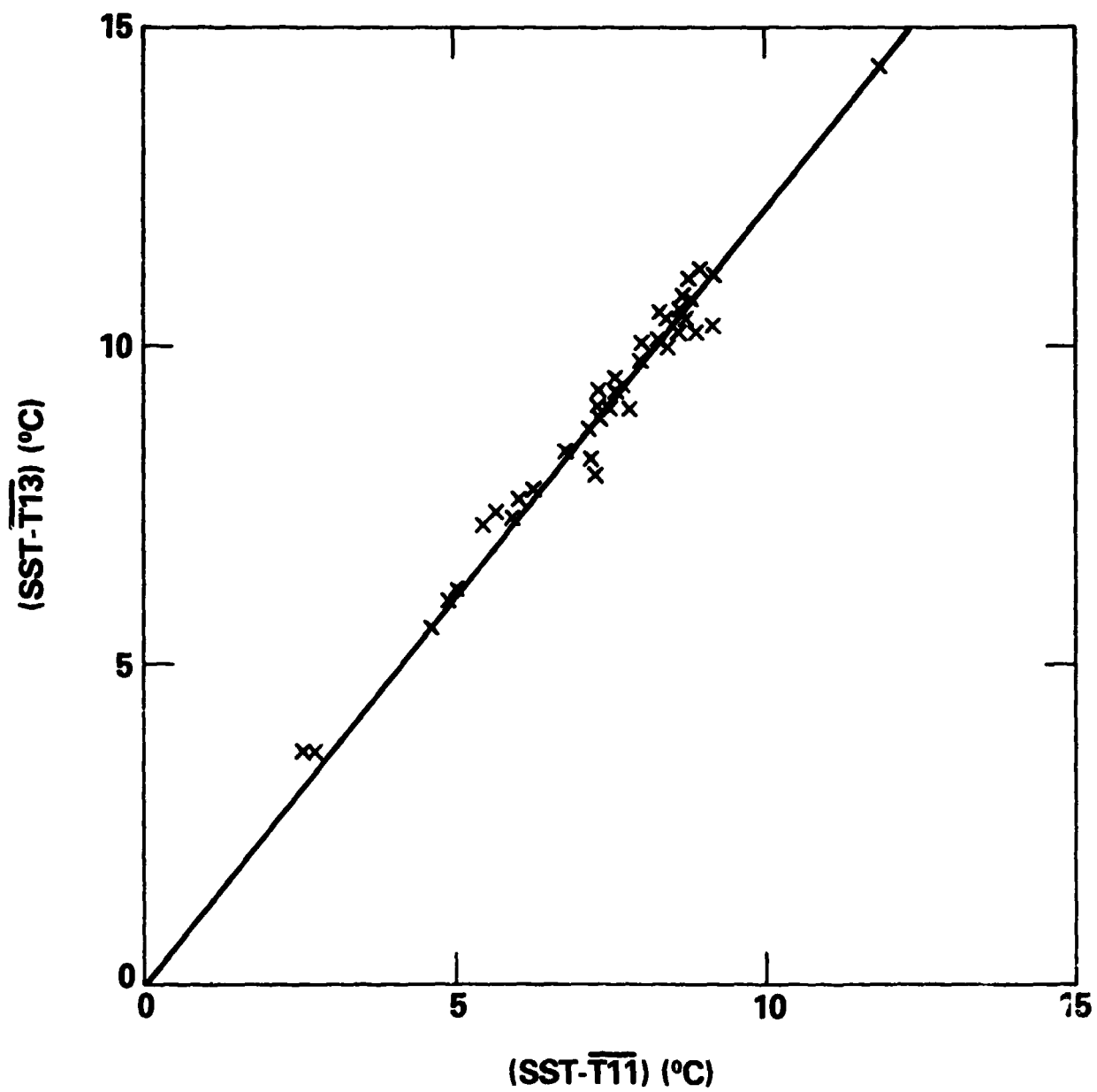
Figure 2. Relationship between the equivalent radiative temperatures for the two window channels at 11 and 13 $\mu$m.
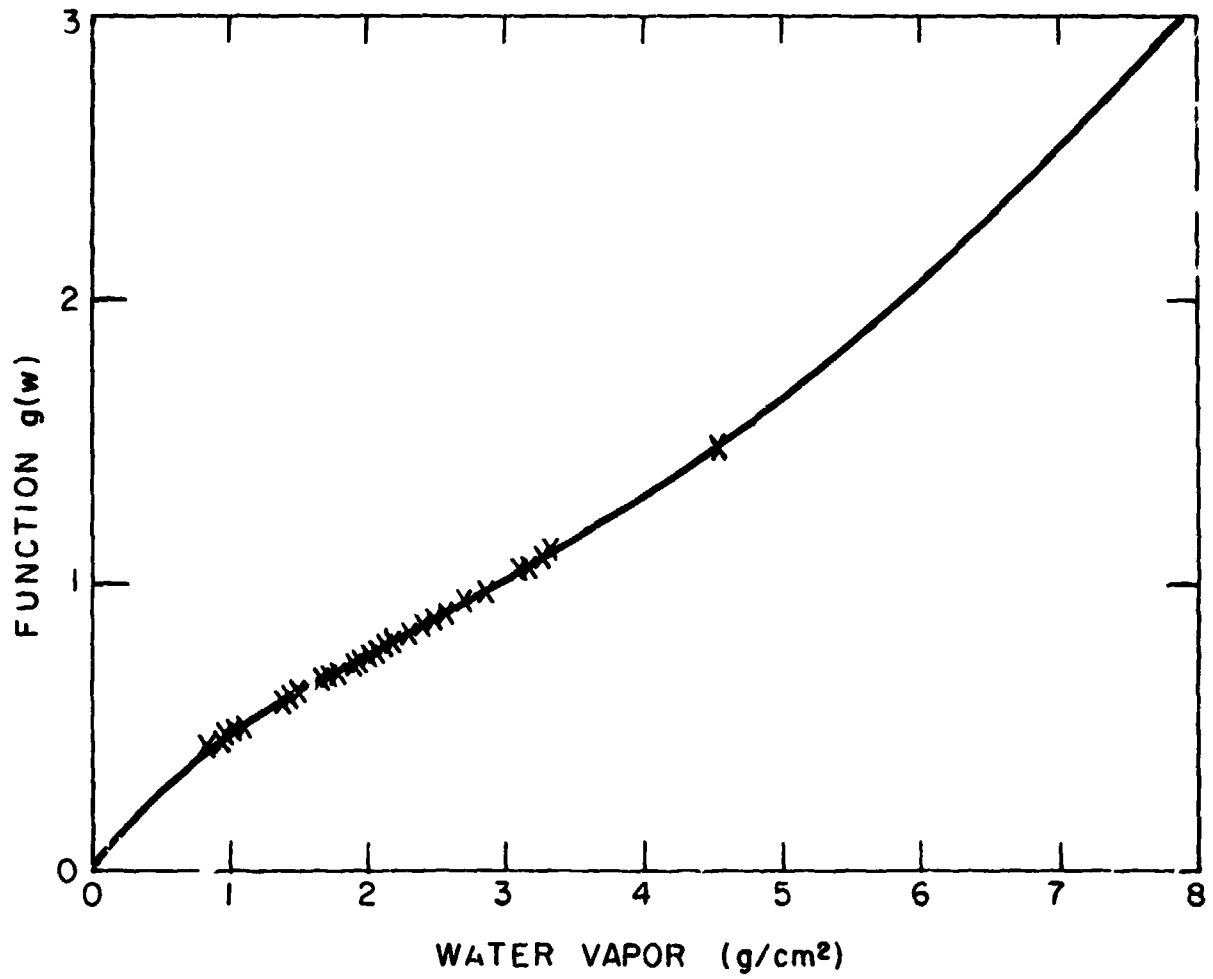
Figure 3. Coefficient for the correction of SST as a function of the total water vapor content.

## THE REMOTE SENSED TOTAL WATER VAPOR CONTENT

The total precipitable water, w, can be obtained from passive satellite measurements in the infrared (Prabhakara et al., 1979), or from measurements in the microwave (Grody, 1978). Comparing the two sources we find that the microwave measurements can be used to secure w in the presence of non-precipitating clouds, but radiometric infrared measurements can be made over a finer field of view. The accuracy in the derived w is about the same.

The water vapor line strength in the 9 $\mu$m window region, was used to derive w with an accuracy better than 0.3 g/cm$^2$ (Prabhakara et al., 1979), provided that spectrometric measurements are available. But radiometric measurements are preferable in operational satellites for their higher accuracy and reliability. For this reason we have examined the possibility of an alternative infrared radiometric measurement to obtain w. The Nimbus 4 IRIS gathered spectral measurements from 400 cm$^{-1}$ to about 1400 cm$^{-1}$ over the globe for a period of about one year (April 1970 to January 1971). The spectral resolution of this instrument is 5 cm$^{-1}$ and the noise equivalent temperature (NET) is about 1°C (Hanel et al., 1972). By using a large sample of IRIS spectra, it was found that the difference between SST and the mean brightness temperature $T_{18}$ in the 18 $\mu$m region, from 496 to 549 cm$^{-1}$, is highly correlated to the 9 $\mu$m line strength.

That is to say w can imply that

$$w = f(T_s - T_{18}) \qquad (10)$$

The simulation model described in the previous section, was applied to 41 radiosonde profiles obtained from oceanographic ships over North Atlantic and North Pacific Oceans, listed in Table 1, to compute $T_{11}$, $T_{13}$ and $T_{18}$. These radiosonde profiles were chosen to correspond to IRIS spectra taken within ±1 degree of latitude and longitude, in nearly cloud-free conditions (Prabhakara et al., 1979). The difference $T_s - T_{18}$ ranges from 10 to 30 K for values of w from

Table 1
Remotely Sensed SST and Results of Radiative Transfer Simulations Calculated from 41 Radiosonde Profiles

| | DAY | SHIP | $(T_s)$SHIP (K) | $(T_s)$SIM (K) | $(T_s - T_{18})$SIM (K) | wSHIP (g/cm$^2$) | wSIM (g/cm$^2$) | g(w) | $(T_s)$IRIS (K) | $(T_{11})$IRIS (K) | $(T_{11})$SIM (K) |
|---|---|---|---|---|---|---|---|---|---|---|---|
| Apr. | 19 | 4 Y M | 277.9 | 277.5 | 14.1 | 0.93 | 1.06 | 0.48 | 273.6 | 271.6 | 277.0 |
| Apr. | 22 | W T K A | 299.4 | 300.8 | 29.3 | 3.82 | 4.55 | 1.50 | 298.6 | 291.8 | 294.0 |
| May | 7 | 4 Y J | 281.0 | 281.1 | 17.1 | 0.91 | 1.43 | 0.61 | 279.1 | 277.4 | 279.9 |
| May | 9 | 4 Y N | 290.9 | 290.9 | 20.1 | 1.90 | 1.90 | 0.73 | 289.2 | 286.7 | 289.2 |
| May | 12 | 4 Y M | 280.1 | 280.2 | 11.4 | 0.99 | 0.80 | 0.45 | 277.7 | 276.7 | 279.5 |
| May | 17 | 4 Y N | 291.5 | 291.5 | 20.9 | 1.93 | 2.00 | 0.77 | 289.0 | 286.7 | 289.6 |
| May | 21 | 4 Y I | 283.7 | 283.6 | 14.2 | 1.58 | 1.06 | 0.49 | 281.3 | 280.1 | 282.7 |
| June | 6 | 4 Y N | 292.9 | 292.9 | 17.5 | 1.72 | 1.48 | 0.62 | 289.0 | 287.1 | 291.5 |
| June | 12 | 4 Y V | 292.7 | 293.3 | 26.2 | 3.46 | 3.31 | 1.11 | 293.8 | 288.4 | 289.9 |
| June | 18 | 4 Y J | 285.1 | 285.1 | 16.7 | 1.35 | 1.38 | 0.59 | 281.3 | 279.6 | 283.8 |
| June | 21 | 4 Y E | 294.4 | 294.4 | 26.0 | 3.71 | 3.23 | 1.09 | 294.4 | 289.6 | 290.2 |
| June | 21 | 4 Y N | 293.1 | 293.1 | 19.1 | 1.73 | 1.69 | 0.68 | 289.8 | 287.7 | 291.6 |
| July | 2 | 4 Y D | 284.9 | 285.1 | 19.3 | 1.82 | 1.71 | 0.68 | 282.5 | 280.3 | 283.7 |
| July | 3 | 4 Y D | 293.1 | 292.9 | 21.1 | 2.80 | 2.04 | 0.78 | 289.8 | 287.8 | 290.9 |
| July | 12 | 4 Y E | 297.7 | 297.5 | 25.7 | 3.50 | 3.15 | 1.06 | 298.0 | 293.1 | 293.8 |
| July | 17 | 4 Y V | 297.9 | 298.4 | 25.5 | 2.64 | 3.09 | 1.05 | 295.2 | 291.3 | 295.4 |
| July | 31 | 4 Y D | 293.3 | 292.7 | 18.9 | 2.58 | 1.65 | 0.67 | 291.9 | 289.4 | 291.0 |
| Aug. | 2 | 4 Y N | 296.1 | 296.2 | 21.5 | 1.83 | 2.10 | 0.79 | 293.8 | 291.2 | 294.0 |
| Aug. | 6 | 4 Y B | 282.7 | 282.7 | 13.7 | 1.18 | 1.02 | 0.48 | 279.7 | 278.6 | 281.9 |
| Aug. | 7 | 4 Y C | 283.7 | 283.7 | 12.9 | 1.78 | 0.94 | 0.47 | 282.3 | 281.0 | 283.0 |
| Aug. | 9 | 4 Y N | 295.9 | 295.9 | 19.9 | 1.74 | 1.82 | 0.72 | 293.8 | 291.3 | 294.1 |
| Aug. | 11 | 4 Y D | 293.5 | 293.2 | 19.3 | 2.07 | 1.72 | 0.69 | 293.0 | 291.0 | 291.6 |
| Aug. | 23 | 4 Y I | 285.1 | 285.6 | 22.8 | 1.72 | 2.36 | 0.86 | 281.8 | 279.7 | 283.5 |
| Aug. | 23 | 4 Y N | 294.7 | 294.6 | 20.3 | 1.88 | 1.90 | 0.74 | 293.5 | 291.1 | 292.6 |
| Aug. | 30 | 4 Y N | 295.9 | 296.1 | 24.6 | 2.54 | 2.82 | 0.98 | 295.1 | 291.9 | 293.1 |
| Aug. | 31 | 4 Y K | 293.2 | 292.9 | 23.4 | 3.25 | 2.53 | 0.90 | 290.1 | 287.3 | 290.1 |
| Sept. | 4 | 4 Y P | 283.7 | 283.4 | 18.6 | 2.65 | 1.64 | 0.65 | 284.4 | 282.3 | 282.2 |
| Sept. | 4 | 4 Y V | 298.7 | 297.8 | 25.8 | 4.14 | 3.18 | 1.07 | 294.8 | 289.8 | 293.8 |
| Sept. | 16 | 4 Y C | 281.9 | 282.1 | 19.6 | 1.37 | 1.77 | 0.71 | 280.7 | 278.7 | 280.5 |
| Sept. | 27 | 4 Y N | 294.1 | 294.0 | 21.5 | 2.27 | 2.10 | 0.79 | 293.8 | 290.9 | 291.9 |
| Oct. | 4 | 4 Y N | 294.9 | 294.7 | 23.1 | 2.46 | 2.44 | 0.89 | 292.3 | 289.2 | 292.2 |
| Oct. | 8 | 4 Y V | 295.3 | 295.7 | 21.7 | 1.50 | 2.13 | 0.80 | 293.4 | 290.9 | 293.7 |
| Oct. | 13 | 4 Y I | 285.9 | 286.4 | 23.5 | 1.87 | 2.53 | 0.91 | 285.8 | 283.0 | 284.0 |
| Oct. | 18 | 4 Y N | 294.9 | 295.4 | 24.0 | 2.08 | 2.65 | 0.94 | 293.5 | 290.6 | 292.9 |
| Oct. | 23 | 4 Y P | 282.1 | 282.3 | 17.3 | 0.83 | 1.43 | 0.61 | 278.3 | 276.8 | 281.2 |
| Oct. | 25 | 4 Y N | 294.3 | 294.4 | 22.4 | 2.12 | 2.24 | 0.83 | 289.3 | 286.7 | 292.1 |
| Nov. | 27 | 4 Y P | 280.9 | 281.0 | 14.2 | 0.91 | 1.05 | 0.49 | 280.7 | 279.3 | 280.1 |
| Dec. | 3 | 4 Y V | 291.3 | 292.0 | 23.9 | 1.58 | 2.62 | 0.94 | 291.1 | 288.0 | 289.7 |
| Dec. | 5 | 4 Y E | 292.9 | 293.4 | 24.6 | 2.09 | 2.82 | 0.99 | 292.0 | 288.8 | 290.6 |
| Dec. | 26 | 4 Y E | 292.7 | 292.5 | 20.5 | 2.01 | 1.94 | 0.75 | 289.8 | 286.8 | 290.6 |
| Jan. | 26 | 4 Y I | 281.5 | 281.6 | 17.8 | 1.12 | 1.50 | 0.63 | 279.5 | 277.8 | 280.3 |

1 to 5 $g/cm^2$. The SST obtained from the split window technique can be used in Equation (10) to derive w, without appreciable degradation of the accuracy. The relationship between $T_s - T_{18}$ and the integrated water vapor content w is shown in Figure 4.

If we use in Equation (10) the relationship shown in Figure 4 values of w can be calculated from $T_{11}$, $T_{13}$, and $T_{18}$. These values are compared with the corresponding ground truth in Figure 5. The error of the water vapor content derived from the 18 $\mu$m brightness temperature is about $\pm0.5$ $g/cm^2$.

The same radiosonde profiles were also used to verify the relationships presented in Figures 2 and 3. The results are shown by the crosses in the same figures.

The brightness temperature $T_{11}$, $T_{13}$, and $T_{18}$ computed for the 41 radiosonde profiles available, were used to estimate the SST. The comparison between the calculated and the measured SST is shown in Figure 6. The error found in this comparison, which is related to the scheme used to obtain SST, is about $\pm0.3^{\circ}C$.
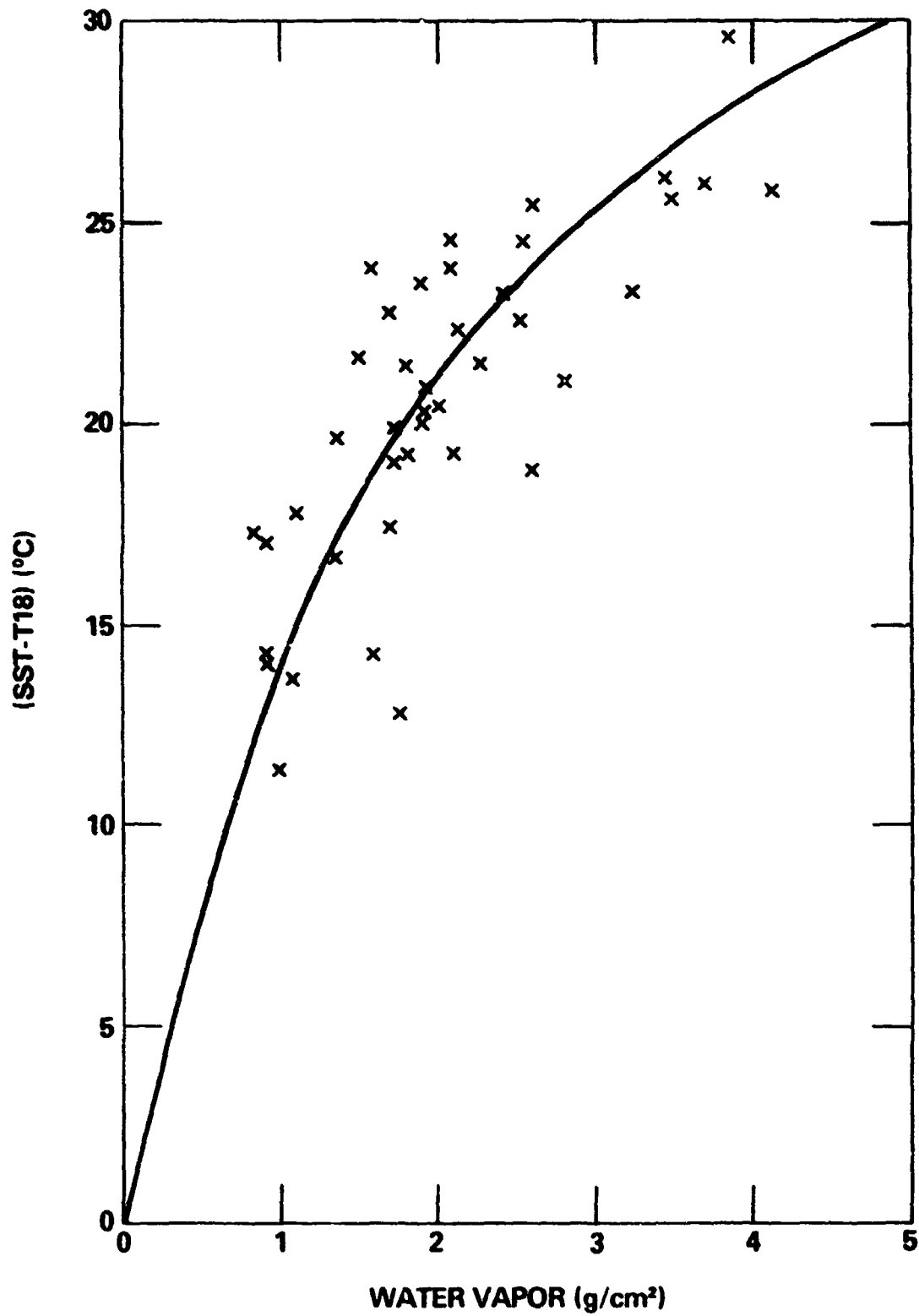
Figure 4. Relationship between the measured water vapor content and the difference SST minus the calculated brightness temperature at 18 μm.
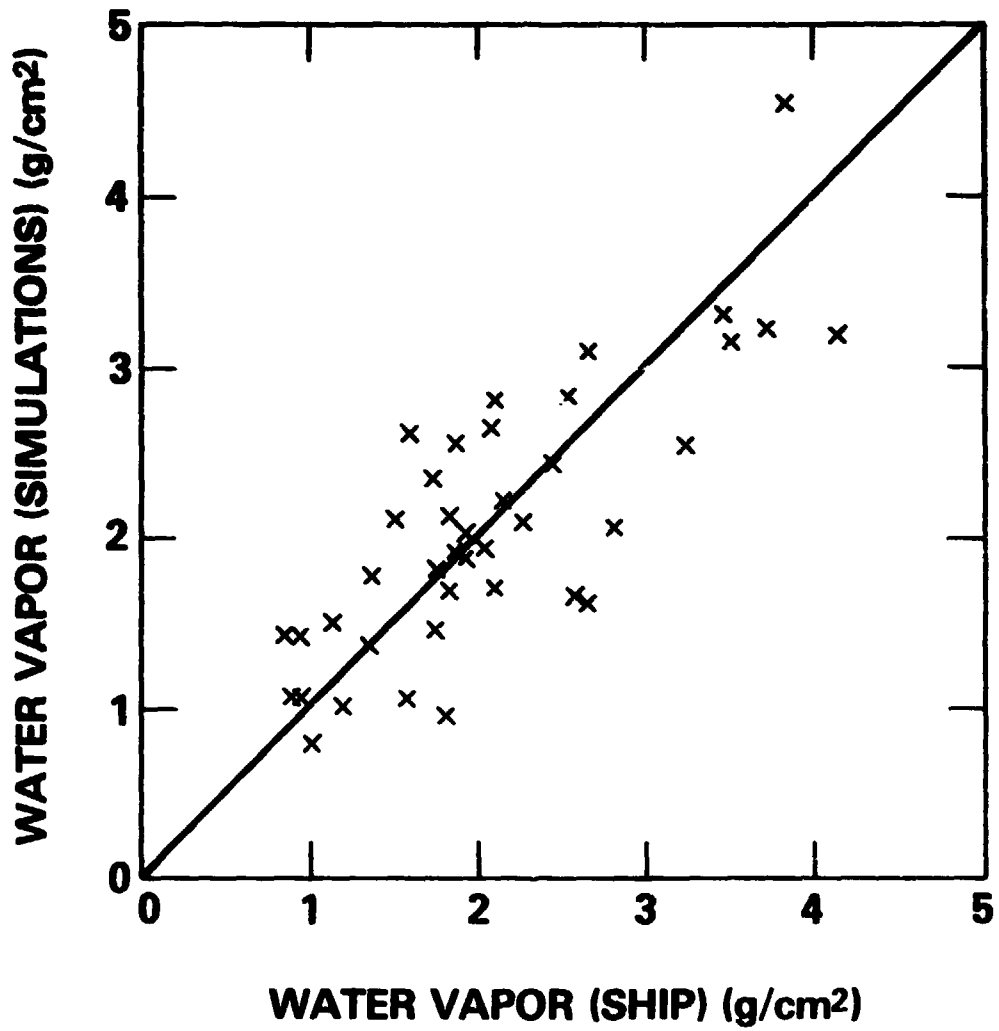
Figure 5. Comparison between the calculated and the observed total water vapor content.
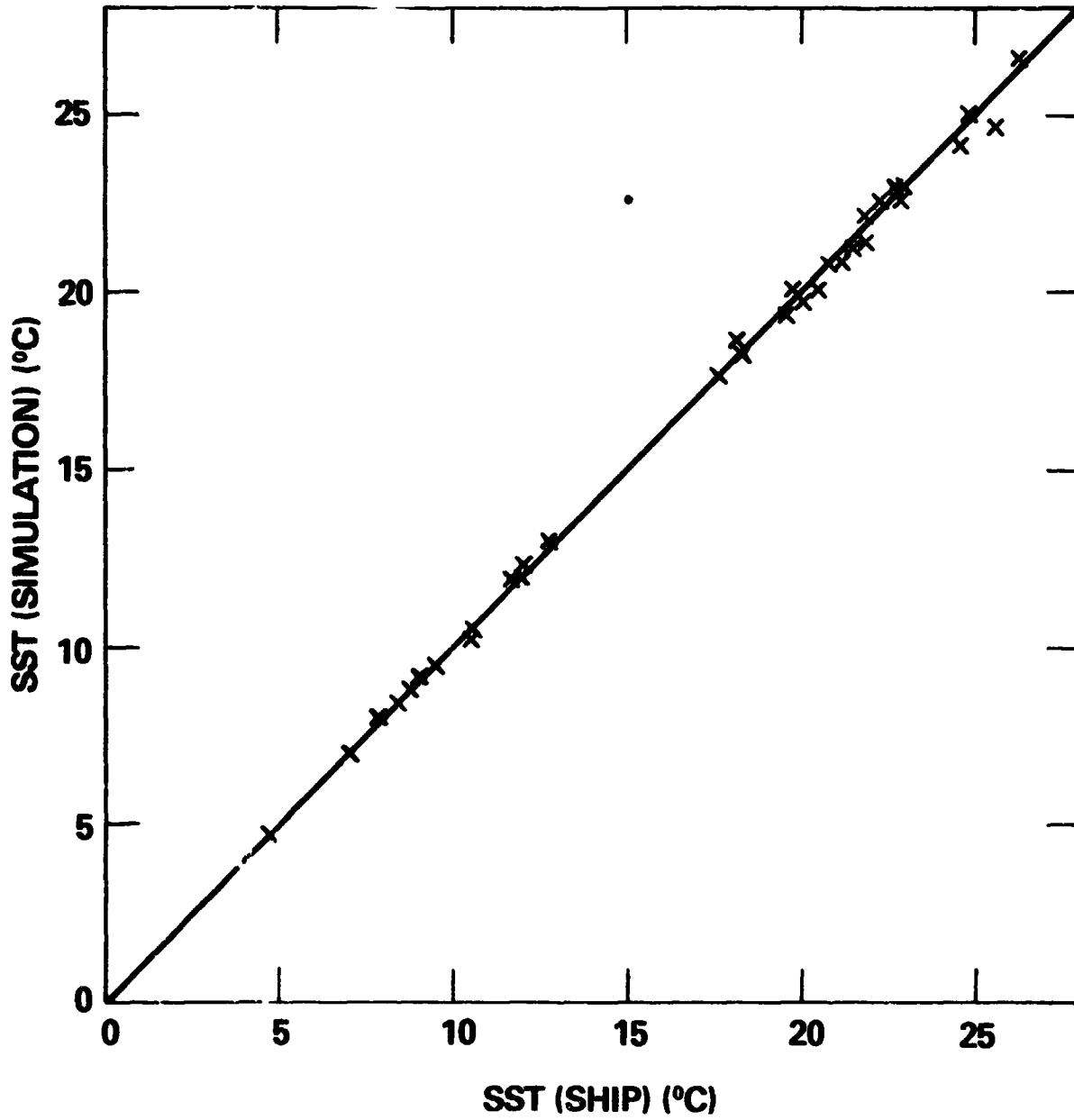
Figure 6. Comparison between the calculated and the observed sea surface temperatures.

## THE EMISSIVITY EFFECT

The emissivity of the surface in the 11 to 13 $\mu$m region is usually assumed to be 1. However, if the accuracy of the SST evaluation has to be of the order of a few tenths of a degree, the effect of the actual surface emissivity should be taken into account.

When the surface emissivity $\epsilon$ $(\nu)$ is less than 1, the complete radiative transfer equation is

$$I(\nu, T) = B(\nu, T_s)\, \epsilon(\nu)\, \tau(\nu, p_0) + \int_{\tau(\nu, p_0)}^1 B[\nu, T(p)]\, d\tau(\nu, p)$$

$$+ [1 - \epsilon(\nu)]\, \tau^2\, (\nu, p_0) \int_{\tau(\nu, p_0)}^1 \frac{B[\nu, T(p)]}{\tau^2\, (\nu, p)}\, d\tau(\nu, p) \tag{11}$$

If we define for convenience a mean atmospheric emission $\bar{B}$, Equation (11) becomes

$$I(\nu, T) = B\ (\nu, T_s)\ E(\nu) + \bar{B}(\nu)\, A(\nu) \tag{12}$$

where

$$E(\nu) = \epsilon(\nu)\, \tau(\nu, p_0)$$

$$A(\nu) = [1 - \tau(\nu, p_0)]\ [1 + (1 - \tau(\nu, p_0))\tau(\nu, p_0)]$$

Now, with the help of the radiative computational scheme previously described, and suitably modified to satisfy Equation (11), we have calculated $I(\nu, T)$, $B(\nu, T_s)$, and $\bar{B}(\nu, \tilde{T})$ for the same atmospheric conditions described in Section 2. The values of the emissivity in the two channels used in our calculations are $\epsilon_{11} = 0.992$ for the 915 to 976 cm$^{-1}$ channel and $\epsilon_{13} = 0.983$ for the 776 to 845 cm$^{-1}$ channel. These values of the emissivity are derived from the data tabulated by Hale and Querry (1973).

In order to combine the equations derived from (12) for two channels, and isolate $T_s$, it is necessary to reduce all the radiances to the same wave length. We have chosen the 11 $\mu$m as reference

wave length, so that

$$B_{13M} (T_s) = B_{11} (T_s) \qquad (13)$$

where $B_{13M}$ indicates that the radiance at 13 $\mu$m has been converted to 11 $\mu$m. After this modification, we find that

$$B_{13M} (T_s) - \bar{B}_{13M} (\bar{T}_{13}) = 1.2[B_{11} (T_s) - \bar{B}_{11}(\bar{T}_{11})] \qquad (14)$$

which is equivalent to Equation (7). Now combining Equation (14) with the equations derived from (12) for the two channels, we have

$$B_{11} (T_s) = \frac{A_{11} B_{13M} (T_{13}) - 1.2 A_{13} B_{11} (T_{11})}{A_{11} E_{13} - 1.2 A_{13} (E_{11} + 0.2 A_{11})} \qquad (15)$$

from which the corrected SST is derived.

The comparison between the measured SST and the SST derived from Equation (15), using the same 41 radiosonde profiles of Section 3, is almost identical to the one presented in Figure 6. In this case the error is also ±0.3°C.

The use of Equation (15) is rather more complicated and time consuming than Equation (8). Since the emissivity effect in the water vapor window region is very low, it was found that, given the same $T_{11}$, the SST corrected for the emissivity effect, can be derived by adding a constant E to Equation (8). The constant E was found to be 0.21 ± 0.07°C for the 41 cases considered.

## COMPARISON BETWEEN SHIP AND SATELLITE MEASUREMENTS

The Nimbus 4 IRIS spectral measurements corresponding to the 41 radiosonde profiles described in Section 3, can be used to simulate the behavior of a three channel radiometer. Then $T_{11}$, $T_{13}$ and $T_{18}$ may be calculated. With the help of these brightness temperatures we can also calculate SST, and compare it with the SST measured by ship. This comparison is presented in Figure 7, and clearly shows that:

a. the remote sensed SST is systematically lower than ground truth,

b. the error is much larger than the one found using the results of the simulations.

However, if we compare the brightness temperature $T_{11}^{IRIS}$ derived from IRIS data and the corresponding $T_{11}^{SIM}$ derived from the radiosonde profiles using radiative transfer model simulations, we find the same bias of the graph presented in Figure 7. In fact the average difference is about 2.6°C. Similar comparison also shows that $T_{13}^{SIM} - T_{13}^{IRIS} \cong 3.4°C$ and $T_{18}^{SIM} - T_{18}^{IRIS} \cong$ 4.3°C. These differences can be compensated if all the radiances measured by IRIS are increased by about 4%. Such a systematic difference between the simulated and the measured IRIS spectra was already noticed by Kunde et al. (1974), and indicates a possible calibration problem in the IRIS instrument.

After compensating for the bias found by adding 4% to all the radiances, an error of 1.5°C is still left in the comparison between the ship measured and the IRIS derived SST (Table 1).

The reasons for such large error are:

a. the existence of some residual cloud contamination in the IRIS data;

b. the poor matching in space and time between ship and IRIS data (the time gap between ships and IRIS can be as much as six hours);

17
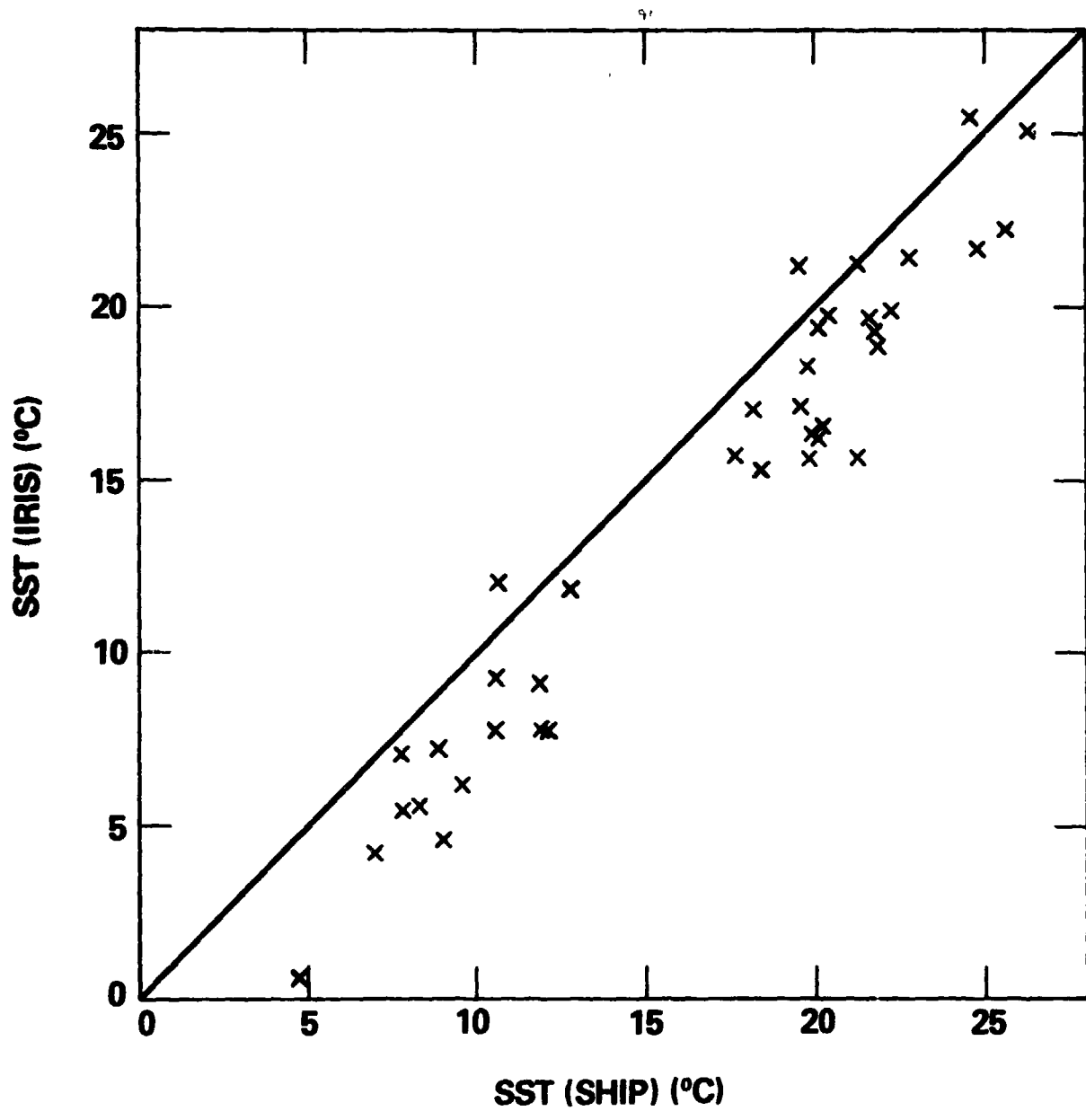
Figure 7. Comparison between the observed sea surface temperature and the sea surface temperature derived from Nimbus 4 IRIS measurements.

c. the radiometric error in the IRIS data;

d. the eɜ  ᵗn the ship measurements equal to about ±1°C (Saur, 1963).

Since all of these errors cannot be eliminated, we are not able at the present time to give a satisfactory ground truth comparison. However we can point out that the comparison between the brightness temperatures $T_{11}^{IRIS}$ derived from the IRIS data and the brightness temperature $T_{11}^{SIM}$ derived from radiosonde profiles with the help of radiative transfer simulations, also show an error of ±1.3°C. In fact, if we eliminate this component, by subtracting from the IRIS de-rived SST, the corresponding $T_{11}^{SIM} - T_{11}^{IRIS}$ values, and if we compare these SSTs with the ship SSTs, we find that the error is reduced to about ±0.5°C.

## CONCLUSION

Sea surface temperature can be calculated to within an accuracy of 1°C (Prabhakara et al., 1974) using the two channels of the TIROS N AVHRR-2 in the 11 to 13 μm water vapor window region. However this accuracy is not sufficient for certain climate models, since sea surface temperature anomalies can produce significant seasonal climatic changes (Namias, 1978; Reiter, 1978). Therefore in this study we have explored the possibility of increasing the accuracy to 0.5°C to meet the requirements of the Climate Program (GARP, 1975).

The SST estimation scheme developed in this study takes into account the atmospheric water vapor absorption and the surface emissivity effect. Radiative transfer model calculations applied to 41 radiosonde profiles taken over the oceans, revealed that the approximations introduced by the present scheme give an error of less than 0.2°C using a water vapor content measured by ships. This error becomes 0.3°C if the error in the remote sensed water vapor content is about 0.5 g/cm$^2$. If PDK's split window technique is used, the error for the same set of data is 0.7°C, and is due primarily to a systematic overestimation of SST.

Since simulations show that the atmospheric absorption correction for SST can be estimated from three channels in the infrared with a relatively high degree of accuracy, the ship measurements of SST for ground truth verification should be taken with the same or better accuracy. Unfortunately such highly accurate measurements are not available at the present time. However an examination of the data available suggests a possible accuracy of about ±0.5°C in the remote sensed SST.

The effect of aerosol scattering is in general negligible when calculating SST. Such aerosol effects are likely to be partially compensated for by the differential absorption scheme in the two channels. Cloud contamination of the data remains the most serious problem. The visible channel

in the AVHRR-2 radiometer can help to minimize the errors due to cloud contamination since its field of view is very fine. Moreover the cloud-contaminated data can be corrected to some extent by comparing radiances measured in adjacent scan spots (Smith, 1968; McMillin, 1978).

# REFERENCES

Bignell, K. J., The Water Vapor Infrared Continuum, Quart. J. Roy. Meteorol. Soc., Vol. 96, 390–403, 1970.

GARP Joint Organizing Committee, The Physical Basis of Climate and Climate Modelling, GARP Publication Series No. 16, pp. 265, WMO, ICSU, 1975.

Grody, N. C., High Resolution Passive Microwave Satellites, Applications to Synoptic Meteorol and Climatology, Application Review Panel Report Chapter 6, Edited by D. H. Staelin and P. W. Rosenkranz, MIT Research Laboratory of Electronics, pp. 6.1–6.40, 1978.

Hale, G. M., M. R. Query, Optical Constants of Water in the 200-nm to 200-$\mu$m Wavelength Region, Applied Optics, Vol. 12, No. 3, 555–563, 1973.

Hanel, R. A., B. J. Conrath, V. G. Kunde, C. Prabhakara, I. Revah, V. V. Salomonson, and G. Wolford, The Nimbus 4 Infrared Spectroscopy Experiment, 1. Calibrated Thermal Emission Spectra, J. Geophys. Res., Vol. 77, 2629–2641, 1972.

Kunde, V. G., and W. C. Maguire, Direct Integration Transmittance Model, J. Quant. Spectrosc. Radiat. Transfer., Vol. 14, 803–817, 1974.

Kunde, V. G., B. J. Conrath, R. A. Hanel, W. C. Maguire, C. Prabhakara, and V. V. Salomonson, The Nimbus E Infrared Spectroscopy Experiment 2, Comparison of Observed and Theoretical Radiances from 425-1450 cm$^{-1}$, J. Geophys. Res., Vol. 79, 777–784, 1974.

Manabe, S., and R. T. Wetherland, Thermal Equilibrium of the Atmosphere with a Given Distribution of Relative Humidity, J. Atmos. Sci., Vol. 24, No. 3, 241–259, 1967.

McMillin, L. M., An Improved Technique for Obtaining Clear Radiances from Cloud-Contaminated Radiances, Mon. Wea. Rev., Vol. 106, No. 11, 1590-1597, 1978.

Namias, J., Multiple Causes of the North American Abnormal Winter 1976-77, Mon. Wea. Rev., Vol. 106, No. 3, 279-295, 1978.

Prabhakara, C., G. Dalu, and V. G. Kunde, Estimation of Sea Surface Temperature from Remote Sensing in the 11 to 13 $\mu$m Window Region, J. Geophys. Res., Vol. 79, No. 33, 5039-5044, 1974.

Prabhakara, C., C Dalu, R. C. Lo and N. R. Nath, Remote Sensing of Seasonal Distribution of Precipitable Water Vapor over the Oceans and the Inference of Boundary Layer Structure, Mon. Wea. Rev., In press, 1979.

Reiter, E. R., The Interannual Variability of the Ocean-Atmosphere System, J. Atmos. Sci., Vol. 35, No. 3, 349-370, 1978.

Saur, J. F. T., A Study of the Quality of Sea Water Temperatures Reported in Logs of Ships Weather Observations, J. Appl. Meteorol., Vol. 2, 417-425, 1963.

Smith, W. L., An Improved Method for Calculating Tropospheric Temperature and Moisture from Satellite Radiometer Measurements, Mon. Wea. Rev., Vol. 96, 387-396, 1968.

Smith, W. L., A Polynomial Representation of Carbon Dioxide and Water Vapor Transmission, ESSA Technical Report NESC-47, U.S. Department of Commerce, National Environmental Satellite Center, Washington D.C., 20 pp., 1969.

Smith, W. L., P. K. Rao, R. Koffler, and W. R. Curtis, The Determination of Sea Surface Temperature from Satellite High Resolution Infrared Window Radiation Measurements, Mon. Weather Rev., Vol. 98, No. 8, 604-611, 1970.

U.S. Standard Atmosphere, 1976, pp. 227, NOAA, NASA, USAF, Washington, D.C., 1976.

Wark, D.Q., J.H. Lienesch, and M.P. Weinreb, Satellite Observations of Atmospheric Water Vapor, Applied Optics, Vol. 13, pp. 507-511, 1974.